Hysteresis in the nonmonotonic electric response of homogeneous and layered unconsolidated sands under continuous flow conditions with water of various salinities, 100 kHz to 2 MHz

M. Kavian,[1] E. C. Slob,[1] and W. A. Mulder[1,2]

Received 31 October 2010; revised 4 May 2011; accepted 18 May 2011; published 27 August 2011.

[1] We measured the electric parameters for four different configurations of unconsolidated homogeneous and layered sands as a function of frequency, water saturation, and salinity under fluid flow conditions. Our objective is to determine if the effect of heterogeneities at scales much smaller than the skin depth can be captured by introducing effective frequency-dependent electrical values whose behavior can be described by simple functions. We employed the parallel plate capacitor technique to measure the complex impedance over a broad frequency range, from 100 kHz up to 3 MHz. We conducted main drainage and secondary imbibition cycles at atmospheric pressure and temperatures between 21°C and 22°C. The hysteretic effect in the real part of the effective complex permittivity at higher concentrations of NaCl is more pronounced for the homogeneous configurations than for the heterogeneous samples. Effective medium theory works well for dry and saturated layered sand, when the NaCl solution concentration is 1 mmol/l. It fails for fully saturated layered sands at salinities of 10 mmol/l or more. It also does not work for partially saturated sands, independent of salinity. A description of the electric properties of a layered sand at all saturation levels by means of an effective homogeneous medium will therefore require a dependence on frequency, saturation level, and salinity of the pore fluid. An extended version of the Cole-Cole model fits the nonmonotonic behavior of the real part of permittivity versus saturation.

Citation: Kavian, M., E. C. Slob, and W. A. Mulder (2011), Hysteresis in the nonmonotonic electric response of homogeneous and layered unconsolidated sands under continuous flow conditions with water of various salinities, 100 kHz to 2 MHz, *J. Geophys. Res.*, *116*, B08214, doi:10.1029/2010JB008083.

1. Introduction

[2] Electric laboratory measurements on unconsolidated sand-water mixtures have shown that the effective complex electric permittivity in the frequency range between 1 mHz and 10 MHz depends on frequency, water saturation level, and salinity [e.g., *Shahidi et al.*, 1975; *Ulrich and Slater*, 2004]. At lower frequencies, between 1 mHz and 10 kHz, spectral induced polarization (SIP) measurements are primarily used to examine polarization of charges near and on mineral-fluid interfaces, as discussed by *Vanhala and Soininen* [1995] and *Breede et al.* [2009], among others. Electric measurements at higher frequencies, between 10 kHz and 10 MHz, were conducted to investigate the electrical behavior of unconsolidated sand under various conditions [*Chen and Or*, 2006]. Experiments were mainly performed on homogeneous, unconsolidated or consolidated sand samples with a static saturation technique, when the pore fluid has reached a static state [*Binley et al.*, 2005; *Schmutz et al.*, 2010]. Those and similar studies mainly focused on the frequency dependence of the electric characteristics.

[3] The key issue, which we are concerned with here, is the electric hysteresis between drainage and secondary imbibition that occurs during continuous fluid flow. In that case, the pore fluid distribution in a heterogeneous porous medium depends on the prior saturation history and can be far from equilibrium. This will appear in the system's electric response, which may show different results for a single value of the saturation. The shallow subsurface, in particular the first few hundred meters, is often subject to sequences of drainage and imbibition due to, e.g., rain and evaporation and changes in the groundwater table. Hysteretic effects also occur for water-immiscible contaminants. Their infiltration and subsequent displacement with, e.g., natural groundwater flow can be determined by electric permittivity versus saturation scanning curves.

[4] *Knight and Nur* [1987a] found hysteresis in the real part of the relative effective complex electric permittivity for sandstone measured at frequencies from 10 kHz to 1 MHz. They started the imbibition cycle by letting dry sandstone samples adsorb water from air at 100% humidity. Higher water saturations were achieved by soaking the samples in

[1]Department of Geotechnology, Delft University of Technology, Delft, Netherlands.
[2]Shell Global Solutions International, Rijswijk, Netherlands.

0148-0227/11/2010JB008083

deionized water. The drainage cycle was performed by simply leaving the saturated samples to dry on the bench top. To achieve low levels of water saturation, samples were placed in a desiccator containing calcium sulfate.

[5] *Longeron et al.* [1989] found hysteresis in the electrical resistivity of two types of strongly water wet samples, sandstone and limestone, when brine and oil saturation was varied during imbibition and drainage cycles. They put the samples between two porous plate electrodes to measure the electrical resistivity at a frequency of 4 kHz.

[6] The electric permittivity hysteresis must be caused by a change in the gradient of the water saturation. This led *Plug et al.* [2007a] to formulate the hypothesis that the difference in water saturation gradient should be measurable in the capillary pressure. They measured nonmonotonic behavior in the real part of the relative electric permittivity for homogeneous and coarse unconsolidated sand as a function of water saturation with distilled water under fluid flow conditions. They also measured hysteresis in the electric response during drainage and imbibition under fluid flow conditions. They found that the capillary pressure was a unique function of the measured electric permittivity and water saturation [*Plug et al.*, 2007b].

[7] We have measured the electric responses, between 100 kHz and 2 MHz, of sand samples under fluid flow conditions, similar to the measurements reported by *Plug et al.* [2007a]. We have done these measurements on unconsolidated homogeneous and layered sands, during drainage and imbibition with air and water of three different NaCl concentrations as saturating fluids, under room temperature and ambient pressure.

[8] The goal is to understand the experiments in terms of effective electric effects that can be used in numerical modeling and inversion of field measurements. For that reason, we investigate to what extent the effective medium theory for layered media holds for measured electric properties of layered sands, using experimentally obtained electric properties of homogeneous sands obtained as a function of frequency, water saturation, and salinity. We further test a simplified version of a double Cole-Cole model to fit the measured data as a function of frequency, for each saturation level and salt concentration. We also investigate the effect of layering on nonmonotonic behavior and hysteresis in electric permittivity and conductivity between drainage and imbibition.

[9] Results of these investigations could be applied to borehole logging data, because the frequency range and physical scale that we use are similar to those used in borehole logging. Modern near surface electromagnetic methods employ a frequency range just below the range considered here [*Moghadas et al.*, 2010]. Such methods lead to considerable sensitivity to soil moisture changes in the vadose zone. For those surface and/or borehole methods there is no scaling issue. For measurements undertaken in the field at larger scales to obtain information for larger depths, downscaling the frequency range by a factor 100 would be necessary. The results could then possibly be applied to these low-frequency surface and/or borehole measurements, which would lead to a discussion about the scalability of the measurements. This is an important issue, because by downscaling frequency we upscale skin depth, but the grain sizes and thereby pore volumes and pore geometries do not scale. A discussion on this subject is outside the scope of the current paper.

2. Experiments

2.1. Experimental Setup

[10] The sample holder, shown in Figure 1, is designed as a flat capacitor, similar to the one used by *Keller and Licastro* [1959], *Mitchell and Arulanandan* [1968], *McCarter* [1984], *Knight and Nur* [1987b], *Shen et al.* [1987], and *Kavian et al.* [2009]. It has an adjustable height and is capable of measuring the electric response, while fluids are flowing through the sample. It consists of two parts: two porous plates, acting as electrodes (SIPERM R80, porous stainless steel), and five PVC rings, each with a diameter of 15 cm and 3 cm height that contain the sample. To avoid water leakage, we use sealing O rings in between the individual PVC rings. These rings are mounted together with Teflon bolts at the top and bottom. A syringe pump (TELEDYNE ISCO pump, 1000D) is connected to the bottom of the sample holder and is set to a constant injection or collection rate with an accuracy of 0.005 ml/min. The sample holder is put in a metallic box that acts as a Faraday cage to shield it from external noise, as illustrated in Figure 1. We use a precision component analyzer (Wayne-Kerr, 6640A) to measure the impedance amplitude, $|Z|$ [Ω], and the phase angle, ϕ [rad], as a function of frequency. These measured values are related to the relative effective complex permittivity, ϵ^*, of the sample, defined by $\epsilon^* = \epsilon_R - \iota\epsilon_I$, where ι denotes the imaginary unit and the indices R and I represent the real and imaginary parts, respectively. We can also use the effective complex electric conductivity, $\sigma^* \equiv \iota\omega\epsilon_0\epsilon^* = \sigma_R + \iota\sigma_I$. These are related by $\sigma_R \equiv \omega\epsilon_0\epsilon_I$, $\sigma_I \equiv \omega\epsilon_0\epsilon_R$, with both ϵ_I and σ_R real nonnegative functions of frequency. Here, ϵ_0 is the permittivity of vacuum and ω is the angular frequency, defined by $\omega = 2\pi f$, f being natural frequency. Note that the sign for the imaginary part depends on the chosen Fourier convention. The opposite choice is obtained by replacing ι with $-\iota$ in the above.

[11] The experimental setup allows measurements at a wide frequency range while fluids flow through the pore volume. We are interested in the electric response behavior as a function of frequency, water saturation, and salinity. We carry out these experiments on homogeneous as well as flat-layered, unconsolidated sand samples. These measurements give the desired effective electric properties of homogeneous and layered sands as a function of frequency depending on water saturation and salinity. The component analyzer is set to output the amplitude $|Z^*|$ (Ω) and phase angle ϕ (rad) of the complex impedance, Z^* (Ω), given by $Z^* = |Z^*|e^{\iota\phi}$. Because the setup is a parallel circuit the relative electric permittivity can be obtained from the measurements as $\epsilon^* = d/(\iota\omega\epsilon_0 A Z^*)$, where d (m) denotes the sample height and A (m^2) denotes the sample cross-sectional area. Statistics of 64 measurements on an air-filled sample holder give us a zero mean amplitude error with a standard deviation of less than 0.2% over the whole frequency range, and an mean phase error of 20 mrad with a standard deviation of less than 1.5 mrad. Because the mean phase error is almost constant over the considered frequency range, we correct for this constant shift and obtain a zero mean phase error with a standard deviation less than 1.5 mrad.

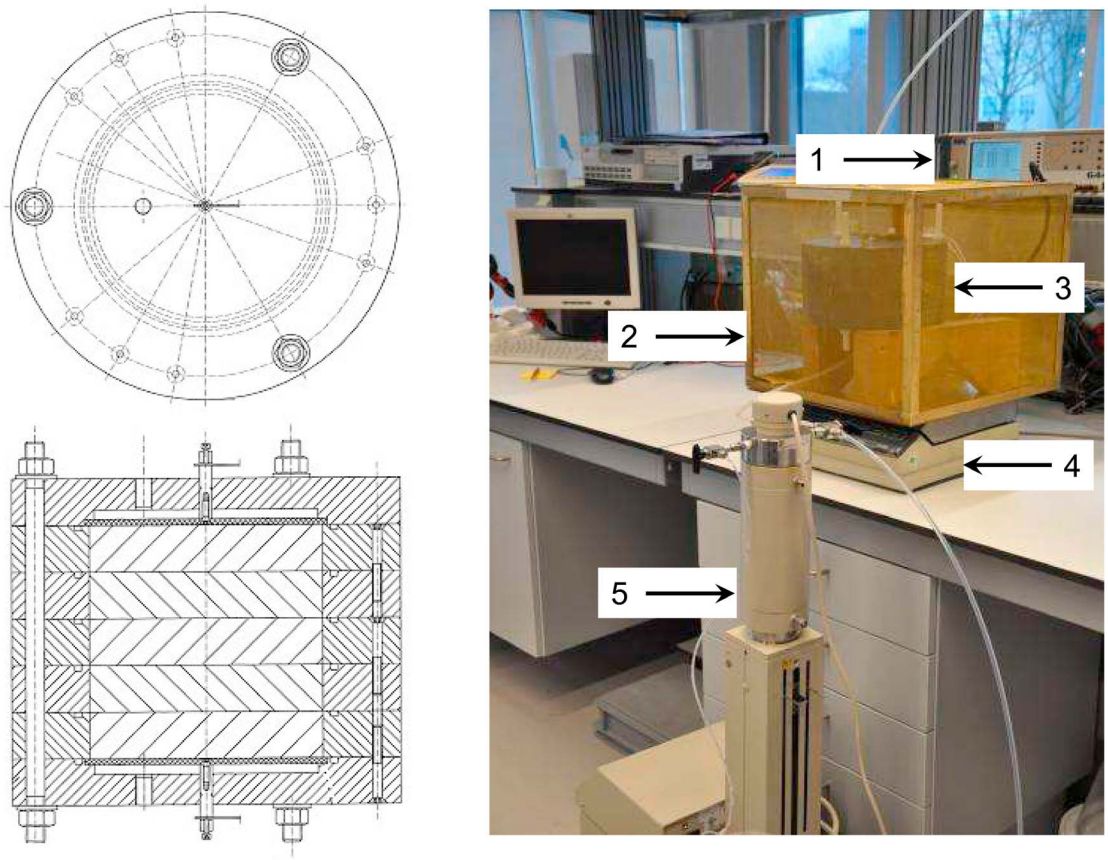

Figure 1. (left) Schematic of the sample holder, consisting of two end pieces, each one containing a porous electrode (SIPERM), air inlet and water inlet at the top and bottom, respectively, and five PVC rings that contain the unconsolidated samples, each ring of 3 cm height and 15 cm diameter. We have used only three of the PVC rings to construct the three-layered unconsolidated sand packs. (right) Experimental set up: 1, component analyzer; 2, Faraday cage; 3, sample holder; 4, balance; 5, ISCO pump.

2.2. Samples and Measurements

[12] We performed experiments on fine- and coarse-grained unconsolidated quartz sand samples. The electrical measurements ran almost continuously during saturation (imbibition) and desaturation (drainage) cycles, for three different concentrations of NaCl in water (1 mmol/l, 10 mmol/l, and 100 mmol/l). The coarse and fine sands had a grain size distribution ranging from 350 μm to 420 μm (D70) and 150 μm to 175 μm (D25), respectively. The untreated sand samples, with a height of 9 cm and a diameter of 15 cm, were placed in the sample holder for measurements.

[13] We considered the two homogeneous samples and two different combinations of a three-layer model. These combinations are sketched in Figure 2. We define homogeneous coarse and fine grain size sands as H350 and H150, respectively. The two layered cases are defined as B350-M150-T350 and B150-M350-T150, where B, M, and T stand for the bottom, middle, and top layers as sketched in Figure 2d. The sample holder was vibrated for 15 minutes to reach a porosity of 0.375 ± 0.005 and 0.395 ± 0.005 for the coarse- and fine-grained sands, respectively. The porosity was calculated with the formula discussed by *Plug and Bruining* [2007]. Then the sample holder was put inside the Faraday cage and filled from the bottom with water of the lowest concentration of salt (primary imbibition) until the sample was fully saturated.

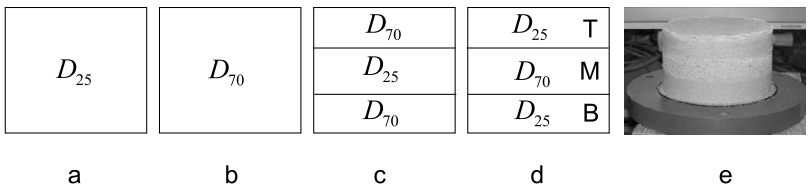

Figure 2. Four different configurations of the sand pack: (a) a homogeneous fine sand; (b) a homogeneous coarse sand; (c and d) three-layer sands with different grain sizes in two geometries; (e) photograph of the three-layered sand sample (B150-M350-T150). The height of each layer is 3 cm, the diameter is 15 cm, and the total height is 9 cm in each configuration.

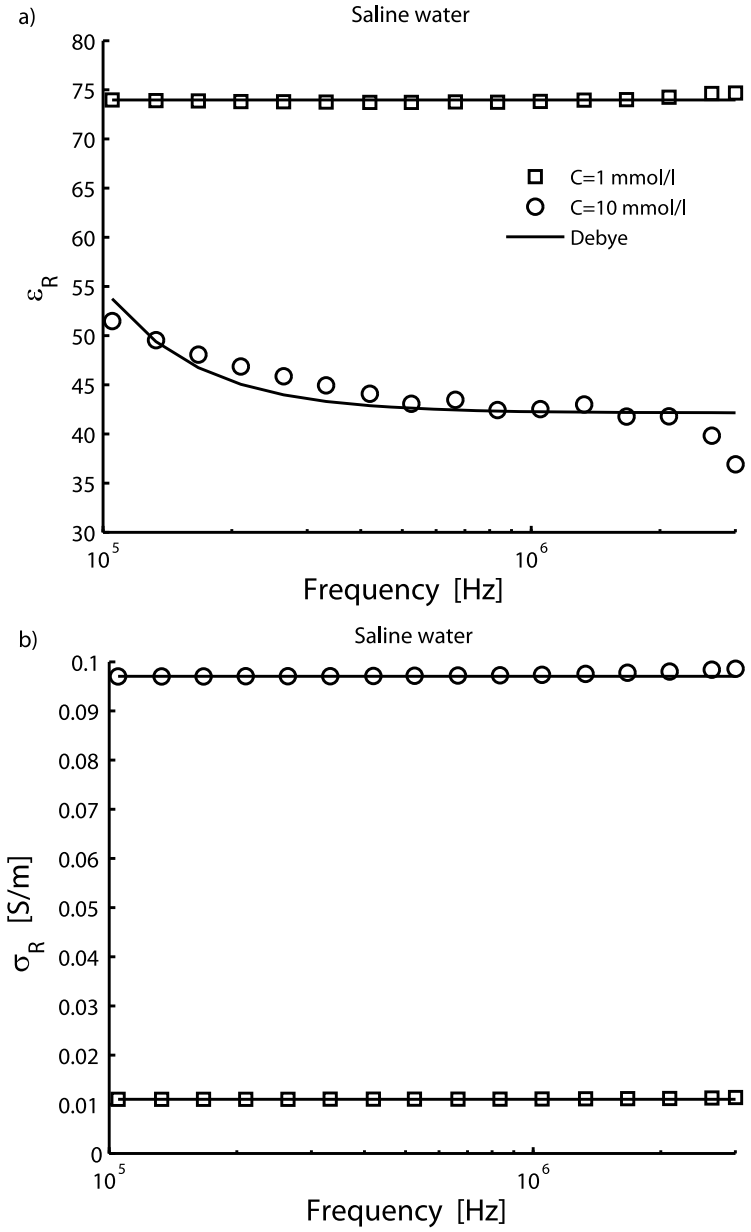

Figure 3. Real part of the electric (a) permittivity and (b) conductivity for saline water with NaCl concentrations of 1 and 10 mmol/l, experimental results (symbols) and model results from *Debye* [1929] (solid lines).

[14] During the next stage, a constant water draining flow rate of 2 ml/min was applied. This main drainage process was continued until air flowed through the sample and no more water was produced. After 10 to 20 minutes to prepare for the reverse cycle, the second imbibition cycle was started by injecting water at the same constant flow rate as used for drainage, using fresh saline water, not the drained fluid. We determined the water saturation from the produced or injected water volume during drainage and imbibition using a balance.

2.3. Data Validation

[15] We analyzed our NaCl solution measurements based on the model of *Debye* [1929]. Similar to the work of *Batalioto et al.* [2010] on dielectric dispersion of water, we fitted our experimental data to Debye's model to validate our NaCl solution measurements. We limited our validation to the case that one relaxation time is enough for a reasonably good description of our NaCl solution measurements. This is a valid assumption since in our NaCl solutions only one group of ions is present, and the cations (Na^+) and anions (Cl^-) have the same mobility [*Barbero and Alexe-Ionescu*, 2005]. Figure 3a shows the measured electric permittivity spectra for two different NaCl concentrations together with Debye's model. The agreement between the experimental data and the model is good with an error of less than 1% for C = 1 mmol/l at each frequency and less than 5% for C = 10 mmol/l at frequencies below 2 MHz. Figure 3b shows the corresponding real parts of the electric conductivity values obtained from the measurements and the

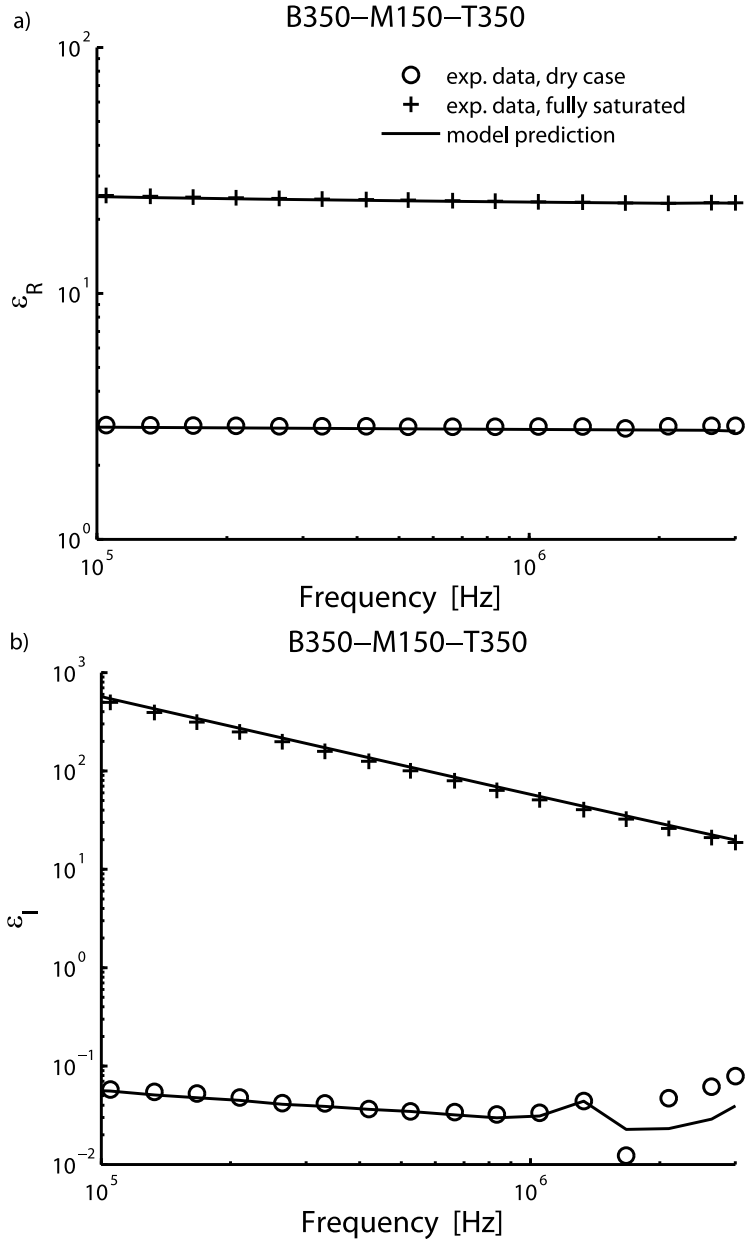

Figure 4. (a) Real and (b) imaginary part of permittivity spectra for the three-layered sand (B350-M150-T350) in the dry (circles) and in the fully saturated case at a NaCl concentration of C = 1 mmol/l (plus signs); the model results according to equation (1) are shown by solid lines.

Debye model. The agreement between the experimental data and the model is very good with an error of less than 1% at each frequency. It can be seen that for a conductivity of 0.01 S/m, the corresponding real part of electric permittivity has a consistent error of 1%, whereas when the value of the real part of conductivity is increased by an order of magnitude the accuracy of the real part of permittivity is decreased to less than 5% at frequencies below 2 MHz. From these results we conclude that we can retrieve real parts of electric permittivity from the impedance measurements with an error of less than 1% when the real part of conductivity is retrieved from the measurements with values less than 0.01 S/m. We have established that our measurements do not suffer from electrode polarization effects in the frequency range from 100 kHz to 3 MHz for all salt concentrations considered. We have also found a bulk conductivity limit of 0.1 S/m below which we can retrieve the real part of conductivity with errors less than 1% and the real part of electric permittivity with errors less than 5%.

[16] Figure 4 shows the spectral data of the effective permittivity ϵ^* together with the effective model prediction results for the three-layered sand (B350-M150-T350) in dry and fully saturated conditions with a NaCl solution concentration of C = 1 mmol/l. The data from the fully saturated sample are obtained under continuous fluid flow conditions just before the drainage cycle starts. We have used the series

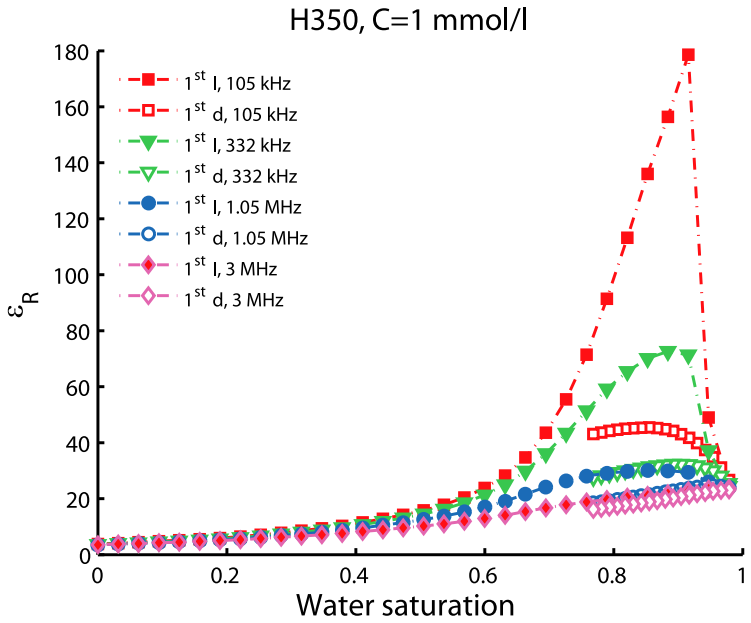

Figure 5. Hysteresis in the real part of the relative effective complex electric permittivity for a homogeneous column of unconsolidated sand with an average grain size of 350 micron at a concentration of C = 1 mmol/l NaCl in water. Data are shown at four different frequencies. Letters *d* and *I* stand for drainage and imbibition, respectively.

capacitors connection model to predict the effective electric permittivity of the three-layered ($n = 3$) sand sample. The general model is given by

$$\epsilon^* = \epsilon_R - \imath\epsilon_I = \frac{1}{\sum_{m=1}^{n} \frac{\psi_m}{\epsilon_m^*}}. \quad (1)$$

Here, ψ_m and ϵ_m^* are, respectively, the volume fraction and the relative effective electric permittivities of layer m obtained from measurements on the corresponding homogeneous samples. The results show that we can substitute an equivalent homogeneous sand for a three-layered dry or fully saturated sand with an error less than 2% for the real and imaginary parts at each frequency. We can also see that the results for the dry sample become less accurate for frequencies above 1 MHz, which was also observed in the measurements on the homogeneous sample. This is because, for an almost nonconducting sample, the limited accuracy of the component analyzer now results in an inaccurate imaginary part of the permittivity. In all further plots we show the real part of permittivity and/or the real part of conductivity computed as $\sigma_R = \omega\epsilon_0\epsilon_I$.

[17] We note that the application of the series connection model to intermediate saturations levels did not provide satisfactory results. This calls for other models to understand measurements at partial water saturation levels. We show model fits in the next section for different saturation levels.

[18] Figure 5 shows the real part of the electric permittivity during the primary imbibition and first drainage cycles with 1 mmol/l salt concentration in water for the homogeneous coarse sand. The primary imbitition measurements are taken with the flow rate set to a constant 1 ml/min. The electric impedance is recorded every 20 minutes until we reach the full saturation level. Then, we decrease the saturation by draining the sample at a flow rate of 2 ml/min. The complete imbibition/drainage cycle takes 16 hours. The excess values of the permittivity increase with saturation during the primary imbibition cycle until a critical saturation level is reached and then drops dramatically. At 105 kHz, the critical saturation level occurs at $S_w = 0.90$ and shifts to lower saturation values at higher frequencies and the effect has vanished at 1 MHz. These results are all consistent with the results from the literature. The significance of these results lies in the fact the first drainage curves always lie below the primary imbibition curves, which is in agreement with the work of *Knight and Nur* [1987b]. We come back to this result in the next section.

3. Experimental Results

3.1. Spectra of Dry Sand Packs

[19] We measured the electrical behavior of the dry sand samples to investigate the effect of grain size, homogeneity, and layering. Figure 6 shows the electric permittivity of the four samples in the initial state prior to the first imbibition. In Figure 6a, the spectra of ϵ_R are independent of frequency. The higher capacitive effect is observed for the layered case (B350-M150-T350) where we have two layers of coarse-grained sand sandwiching a fine-grained sand. In Figure 6b we observe that the real part of conductivity obeys a simple power law as a function of frequency and the values for the mixtures lie in between the values of the homogeneous constituents. Above 1 MHz the accuracy limit of the receiver has been reached.

3.2. Nonmonotonic Behavior of Electric Permittivity as a Function of Water Saturation and Hysteresis in Drainage and Imbibition

[20] Figure 7 shows three plots of the real part of the relative electric permittivity versus water saturation for the

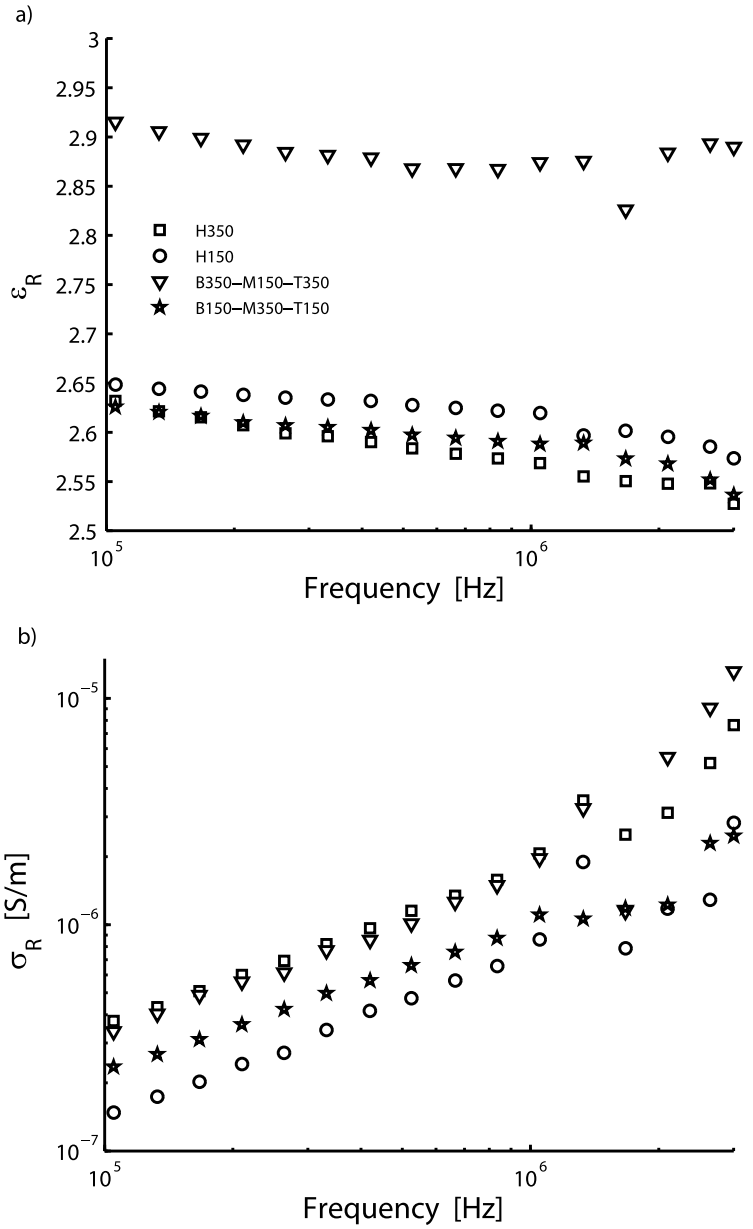

Figure 6. Averaged real part of the (a) relative effective electric permittivity and (b) effective electric conductivity for the four different configurations of unconsolidated dry sand shown in Figure 2.

homogeneous coarse-grained sand at frequencies of 105 kHz, 332 kHz, 1.05 MHz, and 3 MHz, in each plot for a single salt concentration. At the highest concentration of C = 100 mmol/l, the results for 3 MHz are replaced by results for 1.67 MHz, which is the highest frequency where we have accurate data for this salt concentration. Note that the drainage curves are the same in Figures 7a and 5, but the imbibition curves are different. The imbibition curves in Figure 5 are the electric response of a completely dry sample in initial state, where as the imbibition curves in Figure 7a are taken after the primary imbibition and first drainage cycles. In Figure 7a there is a data gap between the saturation level of 0.77 and 0.58 where drainage continues before we switched over to imbibition at saturation level 0.58. Some effect of reversing the flow at partial saturation levels can be observed in all curves.

[21] By comparing Figures 7a, 7b, and 7c it can be observed that for the homogeneous coarse sand sample the nonmonotonic behavior increases with increasing salinity, but decreases with increasing frequency. At the highest salt concentration of 100 mmol/l the nonmonotonic behavior remains strong up to 1.67 MHz as can be seen in Figure 7c. The maximum saturation level we achieved with our technique depends on salinity as can be seen by comparing the rightmost end-points of all open symbols. A second observation is that the difference in saturation after start of first drainage and the end of second imbibition becomes smaller with increasing salinity. At 1 mmol/l salt concentration, the maximum permittivity values at 105 kHz are twice as high

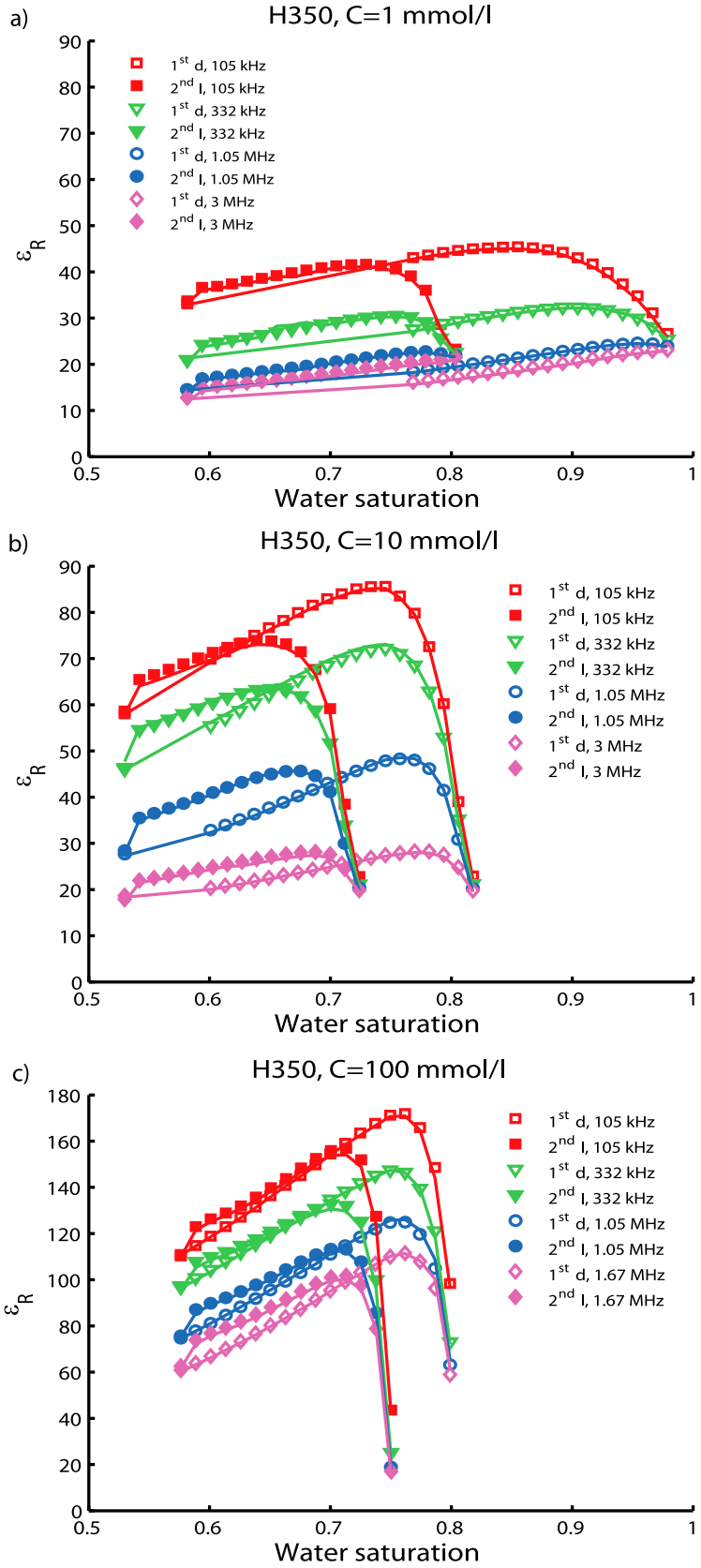

Figure 7. Hysteresis in the real part of the relative effective complex electric permittivity for a homogeneous column of unconsolidated sand pack with average grain size of 350 micron in four different frequencies and (a) C = 1 mmol/l, (b) C = 10 mmol/l, and (c) C = 100 mmol/l NaCl solution concentrations. Letters *d* and *I* stand for drainage and imbibition, respectively. The modeled results are shown by solid lines.

as the maximum values attained at 3 MHz, which is consistent with the work of *Plug et al.* [2007b]. We observe a factor of 4 at 10 mmol/l salt concentration. The curves at 100 mmol/l are relatively closer together than the curves at 10 mmol/l indicating the excess capacitive effect of dissolved charged particles in the pore water depends nonlinearly on salt concentration and the frequency range where this effect occurs becomes wider with increasing salt concentration in the pore water.

[22] We provide a practical model with a small number of fitting parameters to model the complex electric data of unconsolidated sands undergoing continuous drying and imbibing with water of three different salinities. The model is an extended version of the Cole-Cole model [*Pelton et al.*, 1978]. Different forms of extensions have been used by *Ghorbani et al.* [2009] to model the spectral induced polarization of clayey rocks during drying process, by *Weller et al.* [2010] to estimate normalized specific surface area from IP measurements, and by *Kruschwitz et al.* [2010] to investigate textural controls on the electric response of porous media. We assume that the complex impedance contribution of the sample can be described by a parallel circuit of $R_1 - (\imath\omega\chi_1)^{-\alpha}$ which is in series with a parallel classical $R_2 - C_2$ circuit

$$\rho^* = \frac{\rho_1}{1 + (\imath\omega\tau_1)^{\alpha}} + \frac{\rho_2}{1 + \imath\omega\tau_2}, \tag{2}$$

with fitting parameters, ρ_1 and ρ_2 as the resistivities, $\tau_1 = \left(\frac{d}{A}\rho_1\right)^{\frac{1}{\alpha}}\chi_1$ and $\tau_2 = (\frac{d}{A}\rho_2)C_2$ as the relaxation times [*Luo and Zhang*, 1998]. This model (equation (2)) is reproducible from the double polarization model reported by *Kemna et al.* [2000],

$$\rho^*(\omega) = \rho_0\left[1 - \sum_{k=1}^{2} m_k\left(1 - \frac{1}{1 + (\imath\omega\tau_k)^{\alpha_k}}\right)\right], \tag{3}$$

where m_k, τ_k, α_k are chargeability, relaxation time, and dispersion exponent that defines the spread of the relaxation time spectrum. When in equation (3) we take $m_1 + m_2 = 1$, and $\alpha_2 = 1$, we obtain the equation (2) with new fitting parameters, $\rho_1 = m_1\rho_0$, $\rho_2 = m_2\rho_0$. The condition, $m_1 + m_2 = 1$, indicates that the resistivity in zero-frequency limit has the value as ρ_0. This value for the infinite frequency limit becomes zero. The assumption of $\alpha_2 = 1$ reflects a classical parallel R-C circuit. Equation (2) is used to obtain the unknown parameters by fitting the model to the experimental data. The parameters obtained from the fitting procedure, using data for imbibition and drainage, are presented in Tables 1 and 2. The root mean square error (RMSE) is given by

$$\mathrm{RMSE} = \left(\frac{\sum_{n=1}^{N}|d(\omega_n) - d_0(\omega_n)|^2}{\sum_{n=1}^{N}|d_0(\omega_n)|^2}\right)^{1/2}, \tag{4}$$

where N is the number of frequencies, the ω_n are the angular frequencies, d and d_0 are the modeled and experimental data, respectively. The RMSE over the frequency range used here is less than 5% for all saturation levels and salt concentrations. In Table 1, the fitted model parameters for H350 sample are provided for saturations between 0.59 and 0.73 and for three salt concentrations. For the layered sand sample (B150-M350-T150) shown in Table 2, the fitted model parameters were obtained at saturation levels from 0.87 to 0.78 during first drainage and second imbibition cycles, for three salt concentrations. We have a root mean square error of less than 5% for both drainage and imbibition cycles and three concentrations. We use

$$\epsilon_R(\omega) = -\Im\{(\rho^*(\omega))^{-1}\}/(\omega\epsilon_0); \sigma_R = \Re\{(\rho^*(\omega))^{-1}\}, \tag{5}$$

to convert the modeled resistivity values to real relative permittivity and real conductivity and plot the results together with the experimental results to show the goodness of fit.

[23] The modeled results for drainage and imbibition processes are shown in Figures 7 and 8 by solid lines. This model reproduces very well the nonmonotonic behavior observed in the real part of the relative effective permittivity versus saturation, even though for high NaCl solution concentrations the nonmonotonic behavior is more pronounced.

[24] In Figure 8a, the real part of the relative electric permittivity is shown obtained for the three-layered sand (B150-M350-T150) at the lowest salinity. All drainage curves lie above the corresponding imbibition curves. The nonmonotonic behavior for the drainage imbibition cycle at high saturation levels, observed for the homogeneous sand sample at the same salt concentration, does not show up here. At the next NaCl concentration of C = 10 mmol/l, we observe a small hysteretic effect, shown in Figure 8b. Increasing the salinity by another order of magnitude leads to a much stronger hysteretic effect between drainage and imbibition and causes all the drainage curves to drop below the corresponding imbibition curves, as can be seen in Figure 8c. This suggests a change in the capacitive effect of the partially saturated sands as a function of flow direction depending on salt concentration of the pore water. At frequencies below 1 MHz the drainage curves are nonmonotonic, while for frequencies above 1 MHz the drainage curves decrease with increasing water saturation. The imbibition curves increase with increasing saturation for all frequencies.

[25] Figure 9 shows the real parts of the relative effective permittivity versus water saturation at a frequency of 210 kHz, a) for 1 mmol/l, b) for 10 mmol/l, and c) for 100 mmol/l salt concentrations. Each plot shows drainage imbibition results for the three different sand packs, homogeneous sand H350, and the layered sands B150-M350-T150 and B350-M150-B350. The layered sands behave different from the homogeneous sand. The layered sand with the larger coarse-grained fraction is characterized by an imbibition curve that lies above the drainage curve, whereas for the layered sand with the larger fine-grained fraction the imbibition curves lie below the drainage curves for salt concentrations of 1 mmol/l and 10 mmol/l. The homogeneous coarse-grained (H350) unconsolidated sand sample changes its electric response to salinity variations more strongly than the layered sands, whose response is much less affected by a change in salinity.

[26] Figure 10 shows the real electric conductivity values that correspond to the relative real permittivity plots shown

Table 1. Model Parameters for the Homogeneous Sand Sample (H350) Obtained by Fitting the Data for Secondary Imbibition at Three Different Salt Concentrations: C = 1 mmol/l, C = 10 mmol/l, and C = 100 mmol/l[a]

S_w	C (mmol/l)	ρ_1 ($\Omega.m \times 10^2$)	τ_1 (μs)	α	ρ_2 ($\Omega.m \times 10^2$)	τ_2 (μs)	RMSE
0.59	1	5.27	0.07	0.89	0.90	0.98	0.04
	10	0.97	0.01	0.79	0.23	0.23	0.02
	100	0.20	0.09	0.94	0.28	–	0.02
0.64	1	4.70	0.06	0.90	0.78	0.90	0.04
	10	0.31	0.16	0.93	0.69	0.01	0.02
	100	0.16	0.08	0.95	0.23	–	0.01
0.69	1	4.23	0.06	0.90	0.68	0.84	0.04
	10	0.21	0.12	0.93	0.66	0.01	0.02
	100	0.12	0.07	0.95	0.18	–	0.01
0.73	1	3.94	0.06	0.91	0.60	0.78	0.03
	10	0.20	–	0.55	0.33	0.01	0.05
	100	0.07	0.06	0.96	0.14	–	0.02

[a]Saturation levels "S_w" are common between three different salt concentrations. RMSE stands for root mean square error over the frequency range studied here.

in Figure 9. The behavior of the real part of effective electric conductivity versus saturation is shown in Figure 10. Note that the coarse-grained homogeneous sand (H350) has the highest conductivity for all NaCl solution concentrations and the same saturation levels. The electric conductivity imbibition curves for this sample lie above corresponding drainage curves.

[27] At the lowest salinity, the layered sample (B350-M150-T350), behaves much more like the (B150-M350-T150) for low water saturation, but shows a stronger increase in conductivity as the water saturation increases. The imbibition curve for the layered sand sample(B150-M350-T150) has a conductivity almost independent of saturation (see Figure 10a), which could point at the possibility of grain surface counterions migration as cause for bulk conductivity at these low ion concentrations [*Revil et al.*, 1998], whereas all other sands have an appreciable dependence on water saturation and hence their bulk conductivity increases with an increasing number of bulk ions in the pore water.

[28] In Figure 10b obtained at the intermediate salinity, the three different samples stand fairly apart. The hysteretic effect in the electric conductivity is more clear for the homogeneous coarse-grained sand.

[29] At high salinity, the drainage curves for the two three-layered sand samples follow each other and the drainage curve for the (B150-M350-T150) lies above the drainage curve for the (B350-M150-T350), as shown in Figure 10c.

4. Discussion

[30] *Knight and Nur* [1987a] observed a dependence of the (real part of the relative effective complex) electric permittivity on the saturation history for a tight gas sandstone sample. They used a static technique to reach a saturation of 0.85 through humidity adsorption and immersion of dry sandstone samples in deionized water [see *Knight and Nur*, 1987a, Figure 3]. They observed that the real part of the relative effective permittivity depends on frequency. They found the magnitude of the hysteresis to decrease with increasing frequency, with the permittivity values being larger during imbibition than during drainage over a specific range of saturations.

Table 2. Model Parameters for the Layered Sand Sample (B150-M350-T150) Obtained by Fitting the Data for Both the Drainage and the Imbibition Cycles at Three Different Salt Concentrations: C = 1 mmol/l, C = 10 mmol/l, and C = 100 mmol/l[a]

		ρ_1 ($\Omega.m \times 10^2$)		τ_1 (μs)		α		ρ_2 ($\Omega.m \times 10^2$)		τ_2 (μs)		RMSE	
S_w	C (mmol/l)	*d*	*I*	*d*	*I*	*d*	*I*	*d*	*I*	*d*	*I*	*d*	*I*
0.78	1	31.82	40.59	1.85	2.11	0.70	0.67	4.95	3.71	0.10	0.10	0.04	0.05
	10	5.59	6.76	0.10	0.10	0.73	0.73	0.23	0.33	1.36	0.90	0.03	0.03
	100	0.08	0.28	0.02	0.02	0.82	0.84	0.21	0.22	–	–	0.01	0.04
0.81	1	21.20	30.62	1.64	1.94	0.71	0.66	4.55	3.25	0.09	0.10	0.04	0.04
	10	3.27	4.30	0.06	0.09	0.71	0.71	0.19	0.30	0.90	0.70	0.02	0.03
	100	0.05	0.13	0.02	0.02	0.82	0.82	0.16	0.18	–	–	0.02	0.03
0.84	1	14.13	30.30	1.32	2.22	0.72	0.66	3.89	3.21	0.08	0.10	0.03	0.04
	10	0.98	1.45	0.19	0.16	0.77	0.77	1.18	1.09	0.02	0.02	0.02	0.03
	100	0.02	0.09	0.03	0.02	0.82	0.81	0.13	0.16	–	–	0.02	0.02
0.87	1	11.82	30.89	1.18	2.38	0.73	0.66	3.58	3.21	0.07	0.10	0.03	0.03
	10	0.79	0.95	0.17	0.15	0.78	0.78	0.99	0.96	0.02	0.01	0.02	0.03
	100	0.01	0.09	0.05	0.02	0.83	0.81	0.12	0.16	–	–	0.03	0.02

[a]Letters *d* and *I* stand for first drainage and secondary imbibition cycles, respectively. Saturation levels "S_w" are common for both drainage and imbibition cycles. RMSE stands for root mean square error over the frequency range studied here.

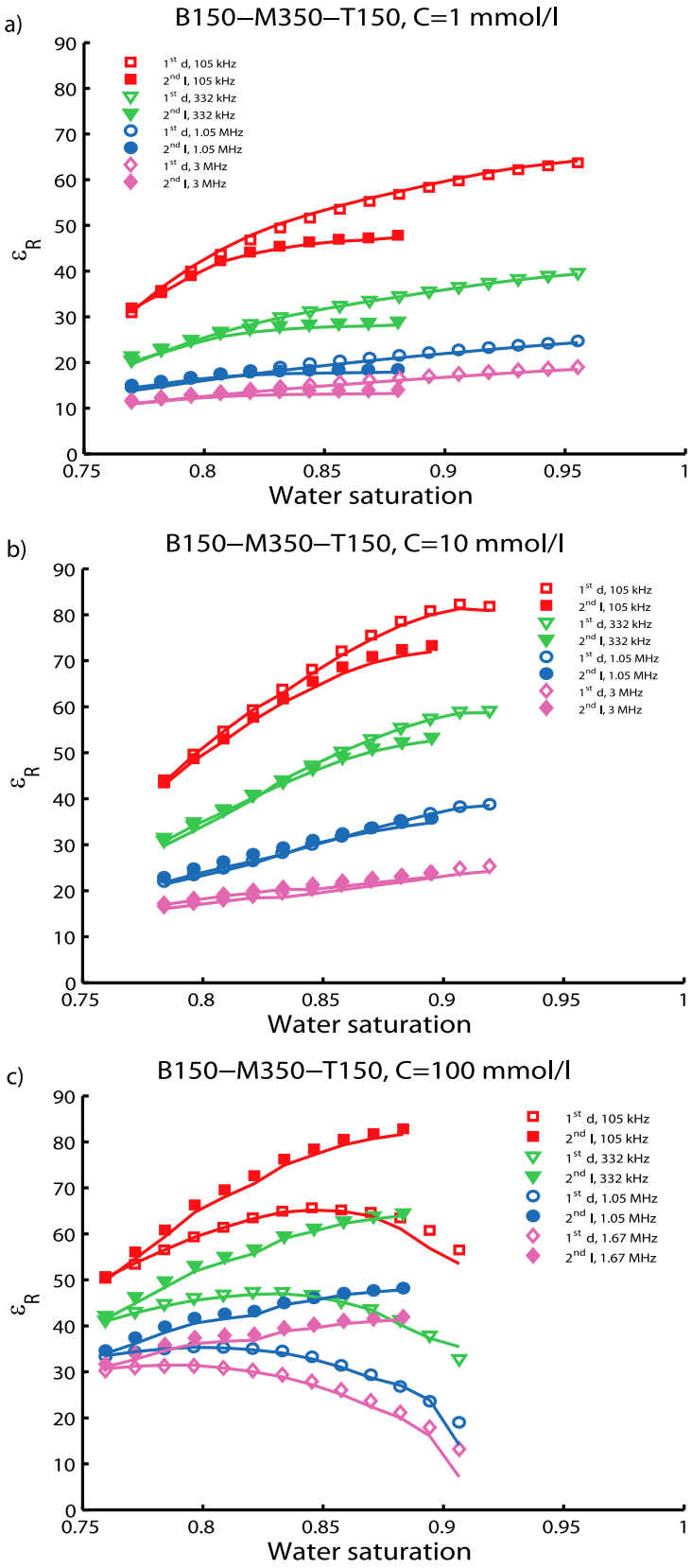

Figure 8. Hysteresis in the real part of the relative effective complex electric permittivity for a three-layered sand pack with average grain sizes of 150 micron at the bottom and top and 350 micron in the middle at four different frequencies and (a) C = 1 mmol/l, (b) C = 10 mmol/l, and (c) C = 100 mmol/l NaCl concentrations. Letters *d* and *I* stand for drainage and imbibition, respectively. The modeled results are shown by solid lines.

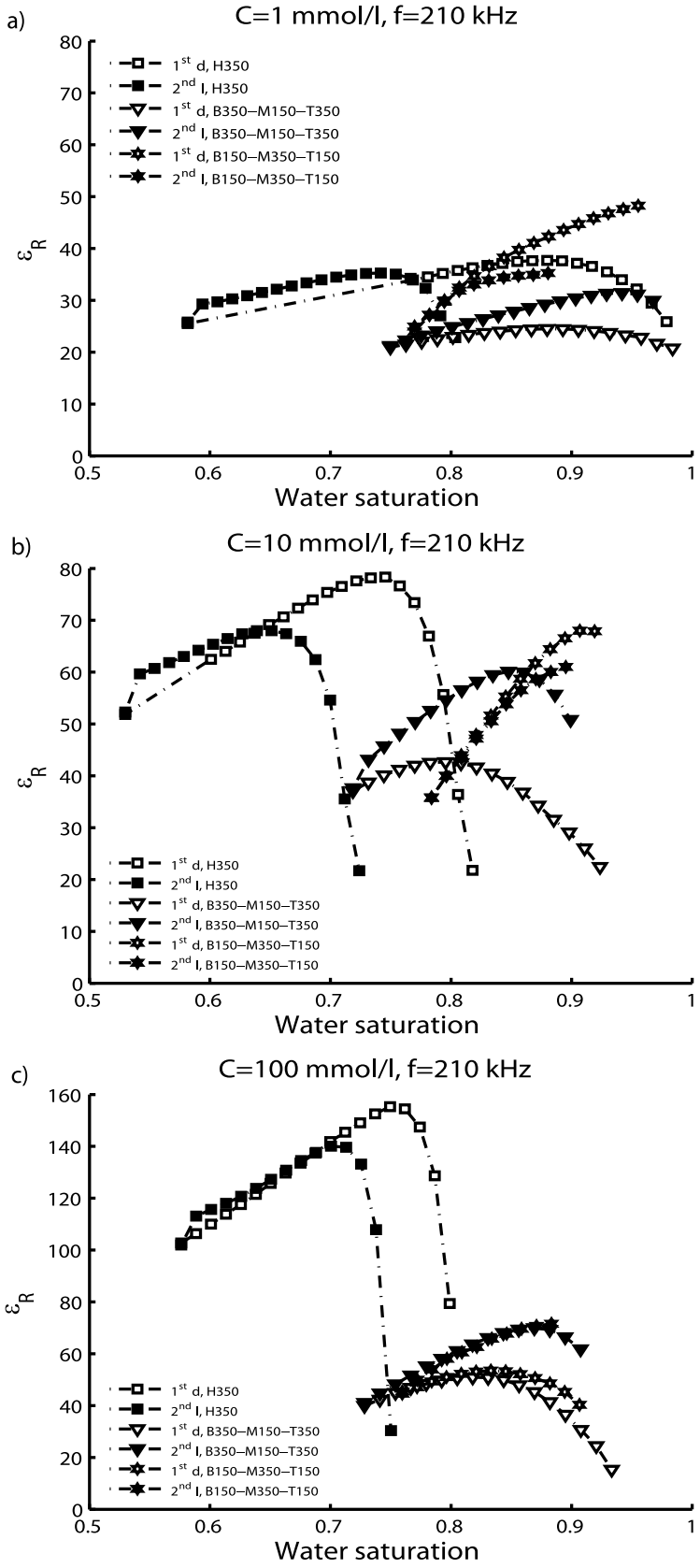

Figure 9. Hysteresis in the real part of the relative effective complex electric permittivity for three different combinations of unconsolidated sand at three different salt concentrations: (a) C = 1 mmol/l, (b) C = 10 mmol/l, and (c) C = 100 mmol/l. The frequency is 210 kHz. Letters *d* and *I* stand for drainage and imbibition, respectively.

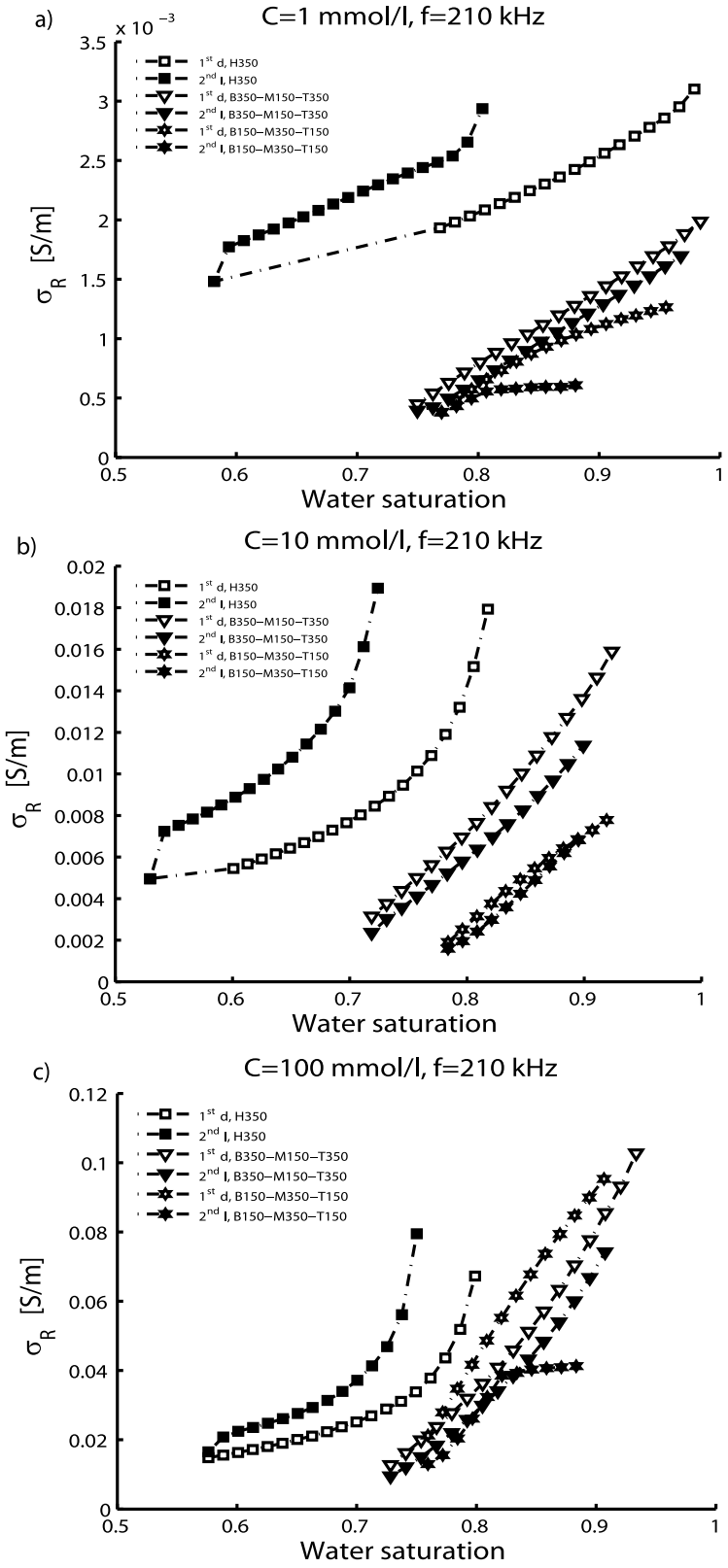

Figure 10. Hysteresis in the real part of the effective complex electric conductivity for three different combinations of unconsolidated sand at three different salt concentrations: (a) C = 1 mmol/l, (b) C = 10 mmol/l, and (c) C = 100 mmol/l. The frequency is 210 kHz. Letters *d* and *I* stand for drainage and imbibition, respectively.

[31] With their static saturation technique, no hysteretic effect were found for frequencies above 105 kHz and for saturations above about 0.7. For imbibition, they observed a critical saturation level above which the permittivity drops. This effect was attributed to a loss of connectivity in the air phase inside the sandstone's pore space. Consequently, the capacitive contribution from the water-air configuration is effectively short circuited. In our dynamic experimental technique, we also observe a critical saturation during drainage, which was not the case in the experiments of *Knight and Nur* [1987a]. Instead, they found a monotonic behavior of dielectric data during drainage, with the permittivity decreasing linearly with decreasing saturation. This effect was interpreted to be due to the fact that a drainage geometry dominates the system after the rearrangement of the pore fluid and the gas phase makes essentially no contribution to the real part of the relative effective permittivity during drainage [*Knight*, 1991].

[32] In our electrical measurements on unconsolidated sand samples, we found a hysteretic effect for frequencies above 105 kHz and saturation levels above 0.7, which not only depends on the frequency but also on the sample configuration and the NaCl solution concentration.

[33] During imbibition, we recorded the electric data under continuous flow conditions until saturation could not be further increased. We saw that under these continuous flow conditions the real part of the relative effective permittivity data of unconsolidated sand samples during primary imbibition are above their corresponding first drainage (see Figure 5). This is consistent with the work of *Knight and Nur* [1987a] on sandstone saturated with distilled water. We continued the drainage imbibition cycles by increasing the NaCl solution concentration and found that the first drainage curves could attain values that are higher than their corresponding secondary imbibition curves. This situation depends on the sample, saturation level, and salinity. It can be reversed for a fine three-layered sand (B150-M350-T150) in highest NaCl solution concentration (see Figures 8c and 9c) or for a coarse three-layered sand sample (B350-M150-T350) for all NaCl solution concentrations (see Figure 9). *Plug et al.* [2007b] reported the same effect in which the scanning drainage curves lie above the corresponding imbibition ones for a CO_2-sand-water system under 8 bar and 13 bar pressure conditions and at 100 kHz.

[34] The observed salinity dependence of the homogeneous and layered unconsolidated sand samples, shown in Figure 9, suggest the possibility to discriminate homogeneous sand samples from layered sands by using saline water in a tracer test [*Slater et al.*, 1997, 2000; *Cassiani et al.*, 2006].

[35] The nonmonotonic behavior in permittivity at a critical saturation threshold can be interpreted using percolation theory as discussed by *Chelidze and Gueguen* [1999]. This theory predicts that, when a continuous conducting path of water is formed, the capacitive contribution from water-air capacitors dies out whereas the water-grain capacitors still have a contribution to the real part of the relative effective permittivity of the sample [*Sen*, 1980]. We experimentally found that the nonmonotonic behavior of the real part of the relative effective permittivity versus saturation becomes more pronounced for high NaCl solution concentrations. A possible explanation for this phenomenon is that the number of the ions increases with increasing concentration and the distance between the ions will decrease. As a consequence, the electrostatic Coulomb interaction between ions will be intensified, which leads to larger values of permittivity.

[36] The highest conductivity observed in all salinities for the homogeneous coarse-grained sand could be due to the high permeability. The most commonly used formula for describing the variation of electric conductivity with saturation S_w, introduced by *Archie* [1942], has the electric conductivity proportional to S_w^n, where n is referred to as the saturation exponent. Figure 10 apparently shows that the variation in electric conductivity with S_w and salinity is more complicated than can be described by Archie's law. The complexity increases when we take the frequency dependence of electric conductivity into account. By fitting the complex resistivity model to the measured data for the homogeneous coarse-grained sand during imbibition at four common saturation levels we can observe significant contribution from the distributed relaxation mechanism. This mechanism is provided in the first part of the model where the shape exponent α can deviate from unity and the results for the homogeneous coarse-grained sand sample are given in Table 1. Values different from unity mean that pore geometry has an influence on the bulk electric resistivity. At all three salinity levels and in the observation range of frequencies the pore water has frequency independent electric resistivity. The dry sand has frequency independent resistivity. When mixed with water the bulk resistivity becomes frequency dependent for the four water saturation levels. At 1 mmol/l salinity concentrations τ_1 and α are fairly constant, at 10 mmol/l τ_1 varies over an order of magnitude, while α increases by more than 10%, from the first to the second saturation levels, then they remain constant when saturation is raised from 0.64 to 0.69, whereas the factor $(\iota\omega\tau_1)^{\alpha}$ becomes irrelevant at the saturation level of 0.73. For the same sample the values that contribute to the classical R-C circuit show a slight decrease, for each salinity level, with increasing saturation level. For each saturation level the resistivity ρ_2 and relaxation time u_2 decrease with increasing salt concentrations and at 100 mmol/l the frequency dependence has disappeared.

[37] From Table 2 we can observe that for the three-layered sand sample (B150-M350-T150) the difference between drainage and imbibition decreases with increasing salt concentration. The shape exponent α increases with increasing salinity and is lower for imbibition than for drainage at 1 mmol/l. Hence effective capacitive effects are more clearly observed at the low salinity of 1 mmol/l. For the part modeling the classical R-C circuit τ_2 is constant during imbibition at 1 mmol/l, whereas it is decreasing with increasing saturation during drainage for both salinity levels where it has significant values and during imbibition at 10 mmol/l. This describes that the effective capacitive effect is reduced at high water saturation levels clearly indicating interplay between water and air in the pore space on the bulk effective frequency dependence of resistivity.

5. Conclusions

[38] Our measurements on homogeneous and layered unconsolidated sand packs for three different NaCl solution

concentrations clearly show that besides the frequency dependence of hysteresis in the real part of the relative effective complex electric permittivity, the hysteretic effects also depend on salinity, macroscopic homogenization of the samples, and the use of a static or dynamic procedure for performing the saturation cycles. Sands under water flow conditions mimic groundwater table variations and subsurface run off during and after precipitation events. Under groundwater flow conditions, sand shows hysteretic electric responses for saturation levels beyond 0.8.

[39] The experiments show that the hysteretic effect in the real part of the relative effective permittivity becomes more pronounced at lower frequencies, at 105 kHz, where the change in interfacial area can be the dominant effect. The hysteretic effect is a function of salinity and the kind of sample. For the homogeneous coarse-grained sand sample, the drainage curves can attain permittivity values that lie above the corresponding imbibition curves whereas this is not the case if the layered sample mostly consists of coarse-grained sands.

[40] For the three-layered sand sample considered in dry and fully saturated case, the measured relative effective complex electric permittivities satisfied the series capacitor model for all frequencies and at low salinities. This implies that the system of layers can be considered as an effective medium or a macroscopically homogeneous mixture.

[41] The five parameter model, which we introduced, very well fits the complex electric resistivity data of homogeneous and layered unconsolidated sands during the drainage and the imbibition cycles under continuous flow conditions and different salinities. For the highest salt concentration of C = 100 mmol/l, a three parameter model is enough to fit the experimental data.

[42] **Acknowledgments.** We thank H.K.J. Heller and F.C. Riem Vis for technical support and Delft Earth and Shell for funding the project. M. Kavian thanks M. Simjoo and M. Miorali for fruitful discussions. We also thank two anonymous referees and the Editor and Associate Editor for their insightful comments and useful suggestions.

References

Archie, G. E. (1942), The electrical resistivity log as an aid in determining some reservoir characteristic, *Trans. Am. Inst. Min. Metall. Pet. Eng.*, *146*, 54–67.

Barbero, G., and A. L. Alexe-Ionescu (2005), Role of the diffuse layer of the ionic charge on the impedance spectroscopy of a cell of liquid, *Liq. Cryst.*, *32*, 943–949, doi:10.1080/02678290500228105.

Batalioto, F., A. R. Duarte, G. Barbero, and A. M. F. Neto (2010), Dielectric dispersion of water in the frequency range from 10 mHz to 30 MHz, *J. Phys. Chem. B*, *114*, 3467–3471, doi:10.1021/jp910114y.

Binley, A., L. D. Slater, M. Fukes, and G. Cassiani (2005), Relationship between spectral induced polarization and hydraulic properties of saturated and unsaturated sandstone, *Water Resour. Res.*, *41*, W12417, doi:10.1029/2005WR004202.

Breede, K., O. Esser, E. Zimmermann, A. Huisman, and A. Kemna (2009), Effects of saturation on spectral induced polarization of sand-clay mixtures, paper presented at International Workshop on Induced Polarization in Near Surface Geophysics, GermanGeophys. Soc., Bonn, Germany.

Cassiani, G., V. Bruno, A. Villa, N. Fusi, and A. M. Binley (2006), A saline trace test monitored via time-lapse surface electrical resistivity tomography, *J. Appl. Geophys.*, *59*, 244–259.

Chelidze, T. L., and Y. Gueguen (1999), Electrical spectroscopy of porous rocks: A review – I. Theoretical models, *Geophys. J. Int.*, *137*, 1–15.

Chen, Y., and D. Or (2006), Effects of Maxwell-Wagner polarization on soil complex dielectric permittivity under variable temperature and electrical conductivity, *Water Resour. Res.*, *42*, W06424, doi:10.1029/2005WR004590.

Debye, P. (1929), *Polar Molecules*, Chem. Catalog Co., New York.

Ghorbani, A., P. C. Cosenza, A. Revil, M. Zamora, M. Schmutz, N. Florsch, and D. Jougnot (2009), Non-invasive monitoring of water content and textural changes in clay-rocks using spectral induced polarization: A laboratory investigation, *Appl. Clay Sci.*, *43*, 493–502.

Kavian, M., E. C. Slob, and W. A. Mulder (2009), Hysteresis in electrical parameters of saline-saturated homogeneous and layered unconsolidated sand, 200 Hz to 3 MHz, *SEG Expanded Abstr.*, *28*(1), 441–445, doi:10.1190/1.3255793.

Keller, G. V., and P. H. Licastro (1959), Dielectric constant and dielectric resistivity of natural-state cores, *U.S. Geol. Surv. Bull.*, *1052–1053*, 257–285.

Kemna, A., A. Binley, A. Ramirez, and W. Daily (2000), Complex resistivity tomography for enviromental applications, *Chem. Eng. J.*, *77*, 11–18.

Knight, R. J. (1991), Hysteresis in the electrical resistivity of partially saturated sandstones, *Geophysics*, *56*, 2139–2147.

Knight, R. J., and A. Nur (1987a), Geometrical effects in the dielectric response of partially saturated sandstones, *Log Anal.*, *28*, 513–519.

Knight, R. J., and A. Nur (1987b), The dielectric constant of sandstones, 60 kHz to 4 MHz, *Geophysics*, *52*, 644–654.

Kruschwitz, S., A. Binley, D. Lesmes, and A. Elshenawy (2010), Textural controls on low-frequency electrical spectra of porous media, *Geophysics*, *75*, WA113–WA123, doi:10.1190/1.3479835.

Longeron, D. G., M. Argaurd, and J. P. Feraud (1989), Effects of overburden pressure and the nature and microscopic distribution of fluids on electrical properties of rock samples, *SPE Format. Eval.*, *4*, 194–202.

Luo, Y., and G. Zhang (1998), *Theory and Application of Spectral Induced Polarization*, *Geophys. Monogr. Ser.*, vol. 8, Soc. Explor. Geophys., Tulsa, Okla.

McCarter, W. J. (1984), The electrical resistivity characteristics of compacted clay, *Geotechnique*, *34*, 263–267.

Mitchell, J. K., and K. Arulanandan (1968), Electrical dispersion in relation to soil structure, *J. Soil Mech. Found. Div. Am. Soc. Civ. Eng.*, *94*, 447–472.

Moghadas, D., F. Andre, E. C. Slob, H. Vereecken, and S. Lambot (2010), Joint full-waveform analysis of off-ground zero-offset ground penetrating radar and electromagnetic induction synthetic data for estimating soil electrical properties, *Geophys. J. Int.*, *182*, 1267–1278, doi:10.1111/j.1365-246X.2010.04706.x.

Pelton, W. H., S. H. Ward, P. G. Hallof, W. R. Sill, and P. H. Nelson (1978), Mineral discrimination and removal of inductive coupling with multi-frequency IP, *Geophysics*, *43*, 588–609.

Plug, W. J., and J. Bruining (2007), Capillary pressure for the sand-CO2-water system under various pressure conditions. Application to CO2 sequestration, *Adv. Water Resour.*, *30*, 2339–2353.

Plug, W. J., E. C. Slob, J. Bruining, and L. M. M. Tirado (2007a), Simultaneous measurement of hysteresis in capillary pressure and electric permittivity for multiphase flow through porous media, *Geophysics*, *72*, A41–A45, doi:10.1190/1.2714684.

Plug, W. J., E. C. Slob, J. van Turnhout, and J. Bruining (2007b), Capillary pressure as a unique function of electric permittivity and water saturation, *Geophys. Res. Lett.*, *34*, L13306, doi:10.1029/2007GL029674.

Revil, A., L. M. Cathles III, and S. Losh (1998), Electrical conductivity in shaly sands with geophysical applications, *J. Geophys. Res.*, *103*, 23,925–23,936.

Schmutz, M., A. Revil, P. Vaudelet, M. Batzle, P. F. Vinao, and D. D. Werkema (2010), Influence of oil saturation upon spectral induced polarization of oil-bearing sands, *Geophys. J. Int.*, *183*, 211–224, doi:10.1111/j.1365-246X.2010.04751.x.

Sen, P. N. (1980), The dielectric and conductivity response of sedimentary rocks, paper 9379, pp. 1–11, Am. Inst. Min. Metall. Pet. Eng., Dallas, Tex.

Shahidi, M., J. B. Hasted, and A. K. Jonscher (1975), Electrical properties of dry and humid sand, *Nature*, *258*, 595–597.

Shen, L. C., H. Marouni, Y. X. Zhang, and X. D. Shi (1987), Analysis of the parallel-disk sample holder for dielectric permittivity measurement, *IEEE Trans. Geosci. Remote Sens.*, *25*, 534–540, doi:10.1109/TGRS.1987.289831.

Slater, L. D., A. Binley, and D. Brown (1997), Electrical imaging of fractures using ground-water salinity change, *Ground Water*, *35*, 436–442.

Slater, L., A. M. Binley, W. Daily, and R. Johnson (2000), Cross-hole electrical imaging of a controlled saline tracer injection, *J. Appl. Geophys.*, *44*, 85–102.

Ulrich, C., and L. D. Slater (2004), Induced polarization measurements on unsaturated, unconsolidated sands, *Geophysics*, *69*, 762–771.

Vanhala, H., and H. Soininen (1995), Labratory techniques for measurement of spectral induced polarization response of soil samples, *Geophys. Prospect.*, *43*, 655–676.

Weller, A., L. Slater, S. Nordsiek, and D. Ntarlagiannis (2010), On the estimation of specific surface per unit pore volume from induced polarization: A robust empirical relation fits multiple data sets, *Geophysics*, *75*, WA105–WA112, doi:10.1190/1.3471577.

M. Kavian and E. C. Slob, Department of Geotechnology, Delft University of Technology, Stevinweg 1, NL-2628 CN Delft, Netherlands. (m.kavian@tudelft.nl)

W. A. Mulder, Shell Global Solutions International, PO Box 60, NL-2280 AB Rijswijk, Netherlands.